Environmental Science Nano



PAPER

View Article Online



Cite this: Environ. Sci.: Nano, 2019, 6, 1688

Emerging investigator series: protein adsorption and transformation on catalytic and food-grade TiO₂ nanoparticles in the presence of dissolved organic carbon†

Junyeol Kim D and Kyle Doudrick D*

The inherent physicochemical properties of engineered nanomaterials (ENMs) are known to control the sorption of proteins, but knowledge on how the release of ENMs to the environment prior to protein exposure affects this reaction is limited. In this study, time-resolved, in situ infrared spectroscopy was used to investigate the sorption of a model protein, bovine serum albumin (BSA), onto two different types of titanium dioxide (TiO₂) ENMs (catalytic-grade P90 and food-grade E171) in the presence and absence of a simple dissolved organic carbon molecule, oxalate. Infrared spectroscopy results showed that oxalate adsorbed to P90 through chemisorption interactions, but it adsorbed to E171 through physisorption interactions due to the presence of inherent surface-bound phosphates. Secondary structure and twodimensional correlation spectroscopy analyses showed that BSA interacted with and unfolded on the surface of P90, but not E171, presumably due to the repulsive forces from the negatively charged phosphates on E171. When oxalate was pre-adsorbed to either P90 or E171, the unfolding of BSA occurred, but along different pathways. This suggests both the "outer" surface chemistry (e.g., oxalate layers) and the mechanism by which this layer is bound to the ENM play a significant role in the adsorption of proteins. Collectively, the results indicate the exposure of ENMs to natural and engineered environments prior to biological uptake affects the resulting protein corona formation, and thus the transport and bioactivity of ENMs.

Received 30th January 2019, Accepted 5th May 2019

DOI: 10.1039/c9en00130a

rsc.li/es-nano

Environmental significance

The protein corona that forms on engineered nanomaterials (ENMs) in biological systems contributes significantly to the bioactivity of ENMs. While the inherent physicochemical properties of ENMs are known to govern formation of the protein corona, there remains a significant knowledge gap on how exposure of ENMs to environments rich in organic matter (e.g., rivers and wastewater treatment plants) prior to biological uptake affects the adsorption of proteins onto ENMs. This work uses time-resolved, in situ vibrational spectroscopy to investigate the protein sorption dynamics on ENMs in the presence of dissolved organic carbon. Outcomes enhance our understanding of how proteins interact with the surface of ENMs that have been exposed to environmentally relevant scenarios.

Introduction

Understanding the interaction of engineered nanomaterials (ENMs) with biological systems is important when considering both its applications (e.g., drug delivery) and implications (e.g., toxicity). Upon contact with biological environments, ENMs can become coated with proteins that form a "corona" around the ENM. While the inherent physicochemical properties of the ENM (e.g., size, surface charge) control the protein sorption behavior, the resulting corona contributes more

Department of Civil and Environmental Engineering and Earth Sciences, University of Notre Dame, Notre Dame, Indiana, 46637, USA. E-mail: kdoudrick@nd.edu

† Electronic supplementary information (ESI) available. See DOI: 10.1039/ c9en00130a

significantly to the behavior of the biosystems. 1-26 Due to their widespread use, ENMs have a high probability of release into the environment throughout their life-cycle. 27,28 To date, most studies on protein corona formation have been conducted using pristine or functionalized surfaces, but there is limited knowledge how ENM exposure to natural and engineered environments prior to biological uptake will affect the protein corona formation.

While the general behavior of the formation of protein coronas on ENMs is known, outcomes are likely to change in realistic scenarios where other macromolecules are present. A critical knowledge gap exists on how the presence of preadsorbed molecules on ENMs will impact formation of the protein corona. Observations from polymer studies have shown the type and size of pre-adsorbed polymers on ENMs

affects the kinetics and composition of the protein corona.29,30 In the environment, inorganic and organic compounds will attach to the surface of the ENM, changing the surface chemistry. For example, the presence of phosphate on titanium dioxide (TiO2) was shown to inhibit the sorption of bovine serum albumin (BSA),31 and organic matter was found to complex with BSA and compete for TiO2 surface sites, altering the protein corona.³²

Environmental Science: Nano

When ENMs enter natural or engineered environments they may interact with ubiquitous dissolved organic carbon (DOC), a complex, heterogeneous mixture of organic compounds in aquatic and terrestrial environments formed through natural degradation processes or exuded from organisms. The physicochemical properties of DOC are source dependent, but generally humic, fulvic, and transphilic acids are the dominant fractions of DOC. 33,34 Humic and fulvic acids are more aromatic, hydrophobic, and have a lower charge density than transphilic acids, and all contain mostly carboxylic and phenolic functional groups.³⁵ These weak acids can adsorb to the ENM surface, effectively changing the transport and reactivity of ENMs in the environment. 36-42 Further, complexation between proteins and DOC is expected to be a significant contributor to the formation of the protein corona.32,43 Thus, the alteration of the surface chemistry of the ENM by adsorbed DOC is expected to change the protein corona's formation behavior.

In this study, real-time, in situ vibrational spectroscopy was used to investigate the adsorption behavior of a model protein, BSA, onto TiO2 ENMs that were exposed to oxalate, a dicarboxylic acid representing a structurally simple DOC. In situ spectroscopy has been successfully used for investigating protein adsorption onto ENMs, 44,45 and it is advantageous for understanding the real-time interfacial behavior. 46,47 To determine the impact of the surface chemistry of the ENM on formation and transformation of the adsorbed BSA, two TiO2 ENMs were investigated: (i) a catalyst-grade TiO2 (P90) and (ii) a food-grade TiO₂ (E171) inherently coated with phosphates. This is the first study to use real-time, in situ spectroscopy to elucidate the formation dynamics and equilibrium of BSA adsorption to TiO₂ ENMs in the presence of DOC. Specifically, this study (i) provides binding information for oxalate and BSA onto P90 and E171 and (ii) knowledge on the effect of pre-adsorbed oxalate on the adsorption behavior of BSA onto P90 and E171.

Materials and methods

Materials

(Photo)catalytic-grade TiO₂ (P90) was obtained from Evonik (Essen, Germany). The average primary particle size of the mixed-phase P90 has been previously reported by our group as 12 nm for anatase (86%) and 18 nm for rutile (14%).⁴⁸ Food-grade TiO2 (E171) was purchased from Minerals-Water Ltd. (Purfleet, UK). BSA (AMRESCO Inc., Solon, Ohio) was used as a model protein in this study (Fig. S1†). Sodium oxalate (Na₂C₂O₄, 99.5+%) purchased from Alfa Aesar (Ward

Hill, MA) was used as a simple DOC surrogate (Fig. S1†). In the environment, oxalate is present from the incomplete oxidation of carbohydrates in plants, and thus serves as a representative simple DOC. All experimental and solution preparations used ultrapure water (Thermo-Barnstead Waltham, MA, 18.2 M Ω cm).

Materials characterization

Transmission electron microscopy (TEM; FEI Titan 80-300, Hillsboro, Oregon) was used to determine the primary particle size and morphology of the ENMs in the presence and absence of BSA and oxalate. The ENMs were mixed with BSA and/or oxalate for 30 min, and then a drop was pipetted onto a carbon-lacey copper TEM grid. Before drying completely, a drop of ammonium molybdate tetrahydrate (2% w/v solution adjusted to pH = 7 with NaOH) was added to provide contrast between the ENM and adsorbed organic layer.

The zeta potential (ζ) and point of zero charge (pH_{zpc}) of P90 and E171 were measured using phase analysis light scattering (PALS, NanoBrook Omni, Brookhaven instrument corporation, Holtsville, NY). To measure the pHzpc, a single stock solution of each TiO2 (0.119 mg L-1) was prepared in 1 mM potassium nitrate (KNO3, Sigma Aldrich ACS Reagent Grade). The stock solution was then split into two samples and the pH adjusted (with HNO3 or NaOH) as needed to measure the ζ at pH values below and above that of the stock solution. After each pH adjustment, the solution was pipetted into a cuvette for subsequent zeta potential analysis. Thirty measurement cycles were conducted at a 15° scattering angle and 25 °C in triplicate for each sample, and the average and standard errors were reported. The zeta potential was calculated from electrophoretic mobilities using the Smoluchowski model (i.e., $\kappa a > 1$). To analyze the effect of BSA and oxalate adsorption, the zeta potential was measured after mixing (t =15 min) with respective concentrations of 3.3 nM and 3.3 μM.

The hydrodynamic size (HDS) and stability of the ENMs was measured in the presence and absence of BSA and/or oxalate using dynamic light scattering (DLS, NanoBrook Omni, Brookhaven Instrument Corporation, Holtsville, NY). Briefly, 5.95 mg L^{-1} TiO₂ was added to either ultrapure water, 0.17 μM of BSA, or 0.17 mM of sodium oxalate, mixed for 15 minutes, and then 3 mL transferred to a cuvette for the DLS measurement. All measurements were conducted at 25 °C with a 10 s equilibration time. The HDS was measured in triplicate at a 90° scattering angle, and the average and standard error of the effective diameters were reported.

Diffuse reflectance infrared Fourier transform spectroscopy (DRIFTS) and X-ray photoelectron spectroscopy (XPS) were used to characterize the surface composition of P90 and E171. DRIFTS analyses were conducted using an EasiDiff accessory (PIKE Technologies, Madison, WI) on a Bruker Vertex 70 FTIR. A 6 mm aperture and 10 kHz scanner velocity were used with a KBr beamsplitter. For each sample, 64 background scans were conducted followed by 64 sample scans of 4 cm⁻¹ resolution from 400 to 4000 cm⁻¹. All spectra were analyzed with OPUS 6.5 software (Bruker Corp., Billerica, MA). XPS (PHI, VersaProbe II) spectra were normalized to the C 1s emission (284.6 eV) and fit using PHI MultiPak software. All samples were analyzed in a window of 124 to 138 eV with a 0.2 eV step size.

Infrared spectroscopy experiments

Adsorption mechanisms of BSA and oxalate onto the ${\rm TiO_2}$ samples were measured using time-resolved, in situ attenuated total reflectance Fourier transform infrared (TRIS-ATR-FTIR) spectroscopy. TRIS-ATR-FTIR experiments were conducted using a Vertex 70 (Bruker Corp., Billerica, MA) equipped with an MCT detector (liquid ${\rm N_2}$ cooled MCT, Infra-Red Associates, Inc., Stuart, FL). The ATR flow-through cell (Pike Technologies, Madison, WI) was outfitted with an AMTIR internal reflection element (IRE) crystal. Spectra were corrected and complemented using functions such as atmospheric compensation and baseline correction available in the OPUS 7.2 software package (Bruker Corp., Billerica, MA).

To create the particulate films on the IRE crystal, TiO_2 solutions (1 g L^{-1}) were prepared in ultrapure water by brief mixing followed by bath sonication for 20 minutes (Branson M3800, 40 kHz). 1 mL of the TiO_2 suspension was evenly distributed on the surface of the AMTIR crystal using a pipette and allowed to dry. The film was then exposed to experimental solutions for analysis. The concentration of TiO_2 was chosen based on outcomes from previous literature^{49,50} and on their acceptable infrared (IR) absorbance intensity observed by us.

TRIS-ATR-FTIR experiments were conducted in either batch or flow-through mode. Batch mode was used to determine the adsorption mechanisms of either oxalate or BSA alone, while flow-through mode was used to simulate changing environments and competitive adsorption of oxalate and BSA. All IR spectra were obtained from 4000 to 800 cm⁻¹ at a 4 cm⁻¹ resolution averaged over 64 scans. To begin, the film was first exposed to water for 20 min to saturate the TiO_2 film with water molecules. This allowed for background water peaks to be removed. In batch mode, the TiO2 film was exposed to either a sodium oxalate (10 mM) or BSA (10 µM) solution for 20 min, and the final time point was reported. For flow-through mode (\sim 6.8 mL min⁻¹), either oxalate or BSA was first flowed across the film for 20 min, followed by flowing the other compound for 20 min (i.e., oxalate followed by BSA). Spectra was recorded approximately every ~8.5 s. After the second compound, water was flowed through the system for 20 min to observe the desorption behavior of the previously adsorbed layers (i.e., oxalate or BSA). All TRIS-ATR-FTIR experiments were conducted one time, and due to natural heterogeneity resulting from the film preparation, some variability is expected and thus the results presented are only semi-quantitative.

Computational analysis of IR data

For the analysis of the BSA secondary structure, the amide I band (1600–1700 cm⁻¹) was extracted and curve-fitted using

Fityk v.0.9.8. 51 Before curve fitting, the background spectra were subtracted from the amide I band followed by atmospheric compensation and baseline correction using OPUS. Goodness of fit was analyzed in-software using χ^2 ; numerous fits were conducted, and the mean and standard deviation values are reported for acceptable fits (<0.0002). Generalized two-dimensional correlation spectroscopy (2DCOS) was used to understand the adsorption dynamics of BSA on TiO₂ in the presence and absence of pre-adsorbed oxalate. 2DCOS is a mathematical tool that can interpret overlapping peaks of IR spectra by spreading the peaks over a two-dimensional array.⁵² For example, it allows the use of spectral intensity to examine the changes in sequential order in the denaturation process of proteins. The major bands and secondary structure of BSA were analyzed using an opensource 2DCOS software, 2D-Shige (Shigeaki Morita, Kwansei-Gakuin University, 2004-2005). In this study, two scenarios were analyzed with 2DCOS for P90 and E171: (1) the BSA spectra with no preadsorbed oxalate, and (2) the BSA spectra with pre-adsorbed oxalate. All spectra data were analyzed following the 2DCOS methods discussed previously.⁵²

Results and discussion

TiO₂ material characterization

The average primary particle size of E171 was previously reported to range from 106–132 nm with a standard deviation of 38–56 nm. TEM images of the E171 sample used in this study showed primary particle sizes within this range (Fig. 1). DRIFTS and XPS analyses indicated the presence of phosphate groups on the surface of the E171 (\sim 2.9% at wt), while no additional surface moieties were observed for P90 (Fig. S2 and S3,† respectively). The pH_{zpc} of P90 and E171 was approximately 6.0 and 4.5, respectively (Fig. 2), which is in good agreement with our previous work on the characterization of different E171 samples. A8,53,54 The lower pH_{zpc} of E171 is attributed to the negatively charged phosphate groups sorbed to the surface of TiO₂. As a result, the zeta potential of E171 remained negative at the experimental pH range used in the study (5.1–6.7), while P90 was mostly positive.

Adsorption behavior of oxalate and BSA onto P90 and E171

IR spectra were collected for oxalate and BSA separately in the absence and presence of P90 or E171 (Fig. 3). The observed IR peak positions for oxalate and BSA are summarized in Table 1. Compared to the solution-phase spectra (*i.e.*, no TiO₂), new peak development and peak shifting upon adsorption may indicate inner-sphere complexation or hydrogen bonding between the adsorbate and adsorbent. The solution-phase peaks for oxalate (Fig. 3a) were assigned to the following vibrations: 1308 cm⁻¹ is CO symmetric stretching [ν_{as} (C-O)], and 1695 cm⁻¹ is CO asymmetric stretching [ν_{as} (C-O)]. The major peaks of the solution-phase IR spectra for BSA (Fig. 3b) were

Environmental Science: Nano

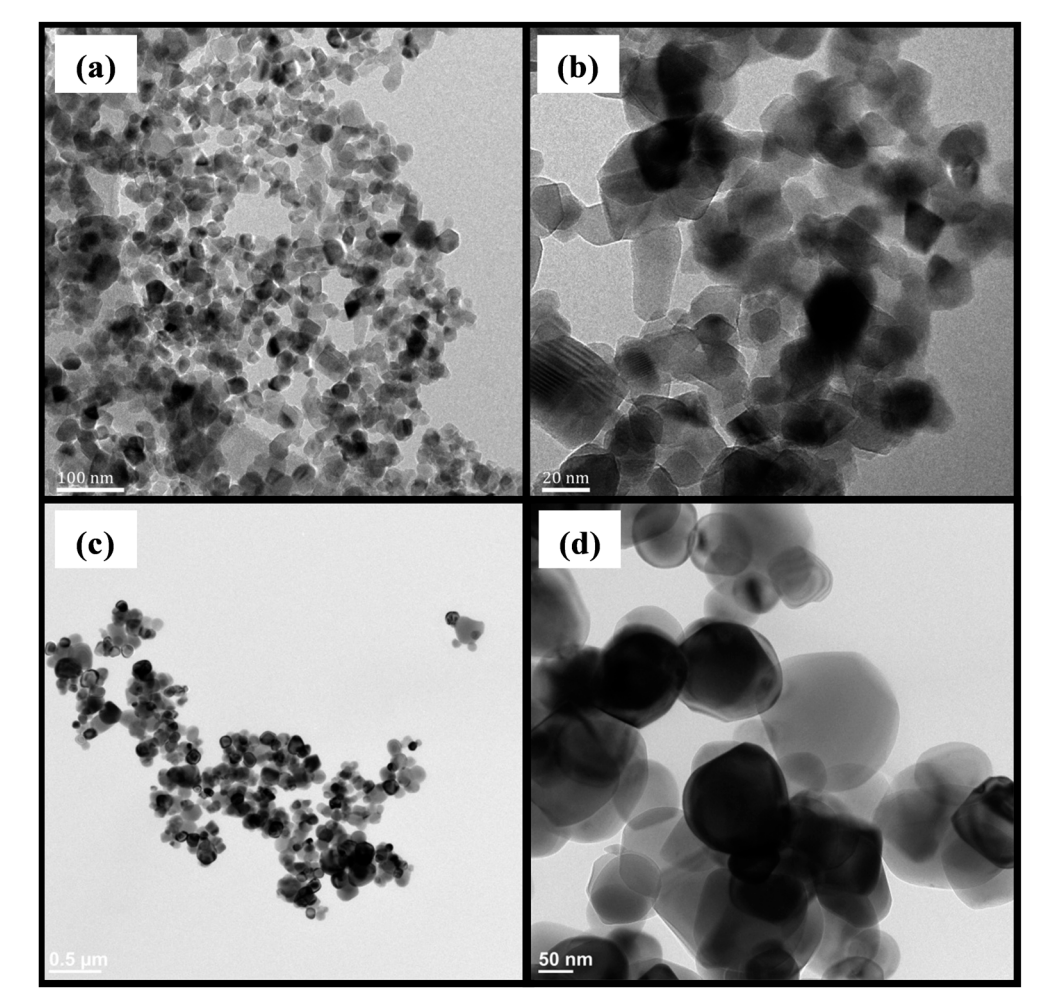


Fig. 1 TEM images of P90 (a and b) and E171 (c and d). Images (b) and (d) are higher magnifications of (a) and (c), respectively.

attributed to the amide I, II, and III bands (1651, 1547, and 1252 cm⁻¹, respectively). The amide I is predominantly CO stretching with contributions from out-of-phase CN stretching, in-plane NH bending, and CCN deformation.⁵⁵

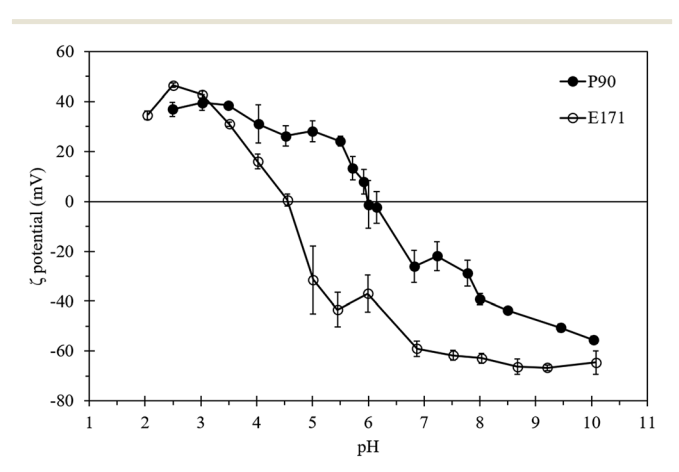


Fig. 2 Average ζ-potentials of P90 (closed circle) and E171 (open circle) as a function of pH. Error bars represent one standard deviation.

The amide II is predominantly out-of-phase in-plane NH bending and out-of-phase CN stretching with contributions from CO bending, CC stretching, and NC stretching.⁵⁵ The amide III is predominantly an in-phase combination of CN stretching and NH bending.55

For oxalate, the mechanism of adsorption differed for P90 and E171 (Fig. 3). For P90, the peak at 1695 cm⁻¹ red-shifted -2 cm⁻¹ while 1566 cm⁻¹ blue-shifted +6 cm⁻¹. These shifts were accompanied by a reduction in the peak intensity for 1566 cm⁻¹ and 1308 cm⁻¹, an increase in the peak intensity for 1695 cm⁻¹, and the formation of two new peaks at 1425 cm⁻¹ [ν (C-O) + ν (C-C)] and 1279 cm⁻¹ [ν _s(C-O) + δ (O-C=O)]. For E171, a shift was only observed for the 1695 cm⁻¹ peak, with a blue-shift of +4 cm⁻¹. Similar to the P90 results, a new peak was formed at 1425 cm⁻¹.

The $[v_s(C-O)]$ and $[v_{as}(C-O)]$ peaks at 1566 cm⁻¹ and 1308 cm⁻¹, respectively, are considered to be weakly adsorbed outer-sphere complexes driven by hydrogen bonds between COO of oxalates and O-H^{δ+} and/or water molecules anchored on the surface of TiO2.56-58 The peaks at 1693-1699 cm⁻¹, 1425 cm⁻¹, and 1279 cm⁻¹ are associated with innersphere complexes between COO and Ti ions of TiO2.58-60

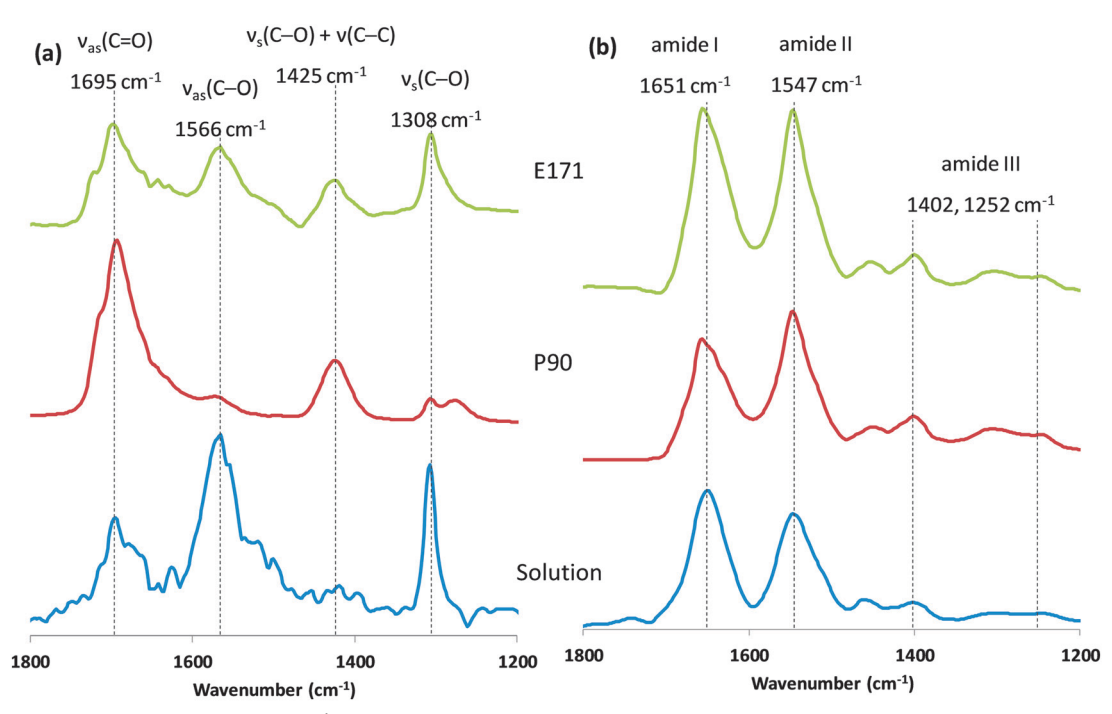


Fig. 3 Batch ATR-FTIR spectra (64 scans, 4 cm⁻¹) of oxalate and BSA in the presence of P90 and E171 films. (a) From bottom to top: Aqueous oxalate, oxalate and P90, oxalate and E171. (b) From bottom to top: Aqueous BSA, BSA and P90, and BSA and E171. The unadjusted pH of samples was 6.7 for oxalate and 5.1 for BSA.

Table 1 Summary of the major IR bands (cm⁻¹) for BSA^{60,88} and oxalate, ^{58,60,86,87} including the solution phase and in the absence and presence of P90 or F171

BSA				Oxalate			
Solution Phase	P90	E171	Assignment	Solution Phase	P90	E171	Assignment
1651	1657	1657	Amide I	1695	1693	1699	$\nu_{as}(C=O)$
1547	1547	1547	Amide II	1566	1572	1566	$\nu_{\rm as}({\rm C-O})$
1402, 1252	1400, 1304, 1248	1400, 1304, 1248	Amide III	_	1425	1425	$\nu_{\rm s}(\text{C-O}) + \nu(\text{C-C})$
				1308	1308	1308	$\nu_{\rm s}({ m C-O})$
				_	1279	_	$\nu_s(C-O) + \delta(O-C=O)$

Thus, P90 conclusively forms an inner-sphere complex with oxalate because of the significant decrease in peak intensity for 1566 cm⁻¹ and 1308 cm⁻¹, the red-shift of 1566 cm⁻¹, the increased intensity for 1693 cm⁻¹, and the formation of new peaks at 1425 cm⁻¹ and 1279 cm⁻¹. For E171, oxalate presumably formed a mixture of outer- and inner-sphere complexes because the physisorption related peaks at 1566 cm⁻¹ and 1308 cm⁻¹ were still present and the chemisorption related peak at 1425 cm⁻¹ was formed. E171 is coated with phosphate groups resulting in a negatively charged surface at the experimental pH (i.e., Fig. 2), and oxalate is also negatively charged at this pH (i.e., HC₂O₄⁻/C₂O₄²⁻). This results in repulsive forces that reduce the transport of oxalate to the surface of TiO2, inhibiting the formation of inner-sphere complexes. However, IR evidence of chemisorption suggests phosphate does not completely inhibit oxalate from entering the inner Stern layer, which is supported by previous reports on competitive sorption between oxalate and phosphate. 61-65 Thus,

either the phosphate does not completely cover the surface or oxalate is able to displace the bound phosphate. The latter is presumably the dominate mechanism as phosphate and oxalate have similar binding constants for TiO2,65 and thus exchange is possible.

For BSA, sorption onto P90 and E171 was apparent as wavenumber shifts were observed for the amide I and III bands and the absorption intensity the amide I/II ratio increased compared to the solution-phase spectra (Fig. 3 and Table 1). This suggests conformation changes of the secondary structure occurred upon adsorption.66-70 The wavenumber shift for the amide I band was identical for P90 and E171, despite their difference in surface chemistry. The blue-shift of the amide I from 1651 to 1657 cm⁻¹ was presumably from the reduction of intramolecular hydrogen bonding and transition dipole coupling of BSA, 69,71,72 resulting from protein unfolding upon adsorption to the TiO_2 .

Though the peak shift of the amide I was identical for P90 and E171, the difference in the amide I shape and the amide I/II ratio suggests the conformational changes upon adsorption were different. Protein adsorption in aqueous solution follows a general three-step process: (1) transport from the bulk to the surface film, (2) attachment to the surface, and (3) rearrangement on the surface, which will change the surface potential and expose different portions of the protein that facilitate further adsorption and structural changes. In an unmixed system, transport is driven by diffusion and is typically the controlling kinetic process.⁷³ Attachment occurs through long- and short-range forces, but long-range forces (e.g., electrostatics) are critical to guiding the protein to favorable sorption sites, whereas immobilization only occurs through strong interactions with the surface.⁷⁴ In our system, the zeta potential of P90 and E171 at the experimental pH of 5.1 was approximately +27.5 and -35 mV, respectively. Thus, at this pH the surface of P90 was composed mostly of Ti- OH_2^+ and Ti-OH groups (i.e., $pH_{zpc} = 6.0$), and E171 was dominated by $H_2PO_4^-$ groups (i.e., $pK_{a1} = 2.15$, $pK_{a2} = 7.20$). The pH_{zpc} of BSA is approximately 4.8 (ref. 75) and thus it would be slightly deprotonated.

Environmental Science: Nano

For BSA sorption to P90, electrostatic attraction between Ti-OH₂⁺ groups and deprotonated moieties on BSA was likely the initial driving force, followed by strong interactions and structural rearrangement upon entering the inner Stern layer. For E171, electrostatic repulsion between negatively charged phosphate groups and deprotonated moieties on BSA suggests transport to the inner layer and chemisorption are not favorable; however, the pHzpc represents the global charge, but BSA consists of a mixture negatively charged (i.e., carboxyl), positively charged (i.e., amino), polar, and nonpolar segments. This results in a complex sorption mechanism that can be spontaneous even in unfavorable electrostatic conditions.⁷⁶ Two modes of attraction are possible: (1) the amino groups were attracted to the negatively charged phosphate groups or (2) non-electrostatic forces between TiO2 and BSA overcame the weak repulsive forces, allowing BSA to attach to the TiO2 surface and then rearrange. Both or one of these mechanisms are possible and have been discussed at length previously for protein adsorption to surfaces;⁷⁶⁻⁸³ however, previous studies have shown phosphate can either complex with BSA^{31,84} or block the adsorption of BSA,⁸⁵ which conflicts with either of the proposed attachment hypotheses. Kinetic and secondary structure analyses were conducted to further elucidate the adsorption mechanism of BSA onto P90 and E171 under varying scenarios.

Sorption kinetics of BSA

The dynamic sorption behavior of BSA in the presence of oxalate was investigated for P90 and E171 under two experimental scenarios: (1) a BSA solution was flowed through the system, followed by an oxalate solution (Fig. 4a and c); (2) an oxalate solution was flowed through the system, followed by a BSA solution (Fig. 4b and d). The purpose of the first scenario was to evaluate the effect of DOC (i.e., oxalate) on adsorbed BSA that was already formed on TiO2 (e.g., a protein coated ENM entering the aquatic environment). The purpose of the second scenario was to investigate how pre-adsorbed DOC affects the adsorbed BSA (e.g., a DOC coated ENM entering the bloodstream). The flow-through experiments are useful since this presents a more realistic scenario (e.g., a lake that has a pseudo-constant high concentration of DOC compared to the protein). For both scenarios, an additional phase was conducted at the end to investigate desorption behavior by water. The C=O and amide II vibrations were selected as representative bands for oxalate and BSA, respectively. The amide II band is good for monitoring and quantifying protein adsorption because it is less sensitive to structural changes and has less interferences from the absorbance of the water band at \sim 1640 cm⁻¹. 30,49,50

The IR absorbance values of BSA and oxalate adsorption onto P90 were approximately an order of magnitude greater than E171 (Fig. S4†) because of the greater available surface area per mass for P90 and more favorable sorption mechanism (i.e., chemisorption). To equally compare the kinetics between samples, the absorbance values were normalized to the maximum observed value for each phase (e.g., for the BSA phase in Fig. 4a, all values were normalized to 0.301).

The Elovich, pseudo zero-order (PZO), pseudo first-order (PFO), pseudo second-order (PSO), and parabolic diffusion models are commonly used to empirically fit sorption data.89-92 None of these models were found to accurately describe any of the BSA adsorption (i.e., to P90 and E171 in the presence and absence of pre-adsorbed oxalate) datasets across all time points, indicating the presence of different sorption mechanisms. Heterogeneous sorption reactions are not easily described by a single kinetic model, and often sorption reactions are modeled without consideration of early, diffusion driven timepoints. 91,93 Schmidt et al. 49 found the simplified Elovich and PSO models to fit the adsorption of BSA to montmorillonite, but early time points in the Elovich model were not predicted well, suggesting diffusional control in this region. In our study, we found a mixture of PZO and PSO models at early and late times, respectively, described the data well ($R^2 > 0.99$, data not shown). The is presumably due to the mixture of sorption mechanisms involved with protein adsorption including physisorption, chemisorption, and structural rearrangement. These empirical kinetic models generally lead to "good fits" because early and late times do not skew the correlation significantly. Because of the complexity of the sorption mechanisms, the inconsistency in the models used to obtain rate constants, and the variability from a lack of experimental repetitions, we instead report the initial slopes of the sorption kinetic curves to gain a general understanding of the behavior. The normalized absorbances were used to calculate the initial rates of adsorption for BSA and oxalate, which corresponded to the initial linear slope of the datasets.

For the first scenario, the initial rates of adsorption of BSA onto P90 (Fig. 4a) and E171 (Fig. 4c) were 0.106 and 0.235 a.

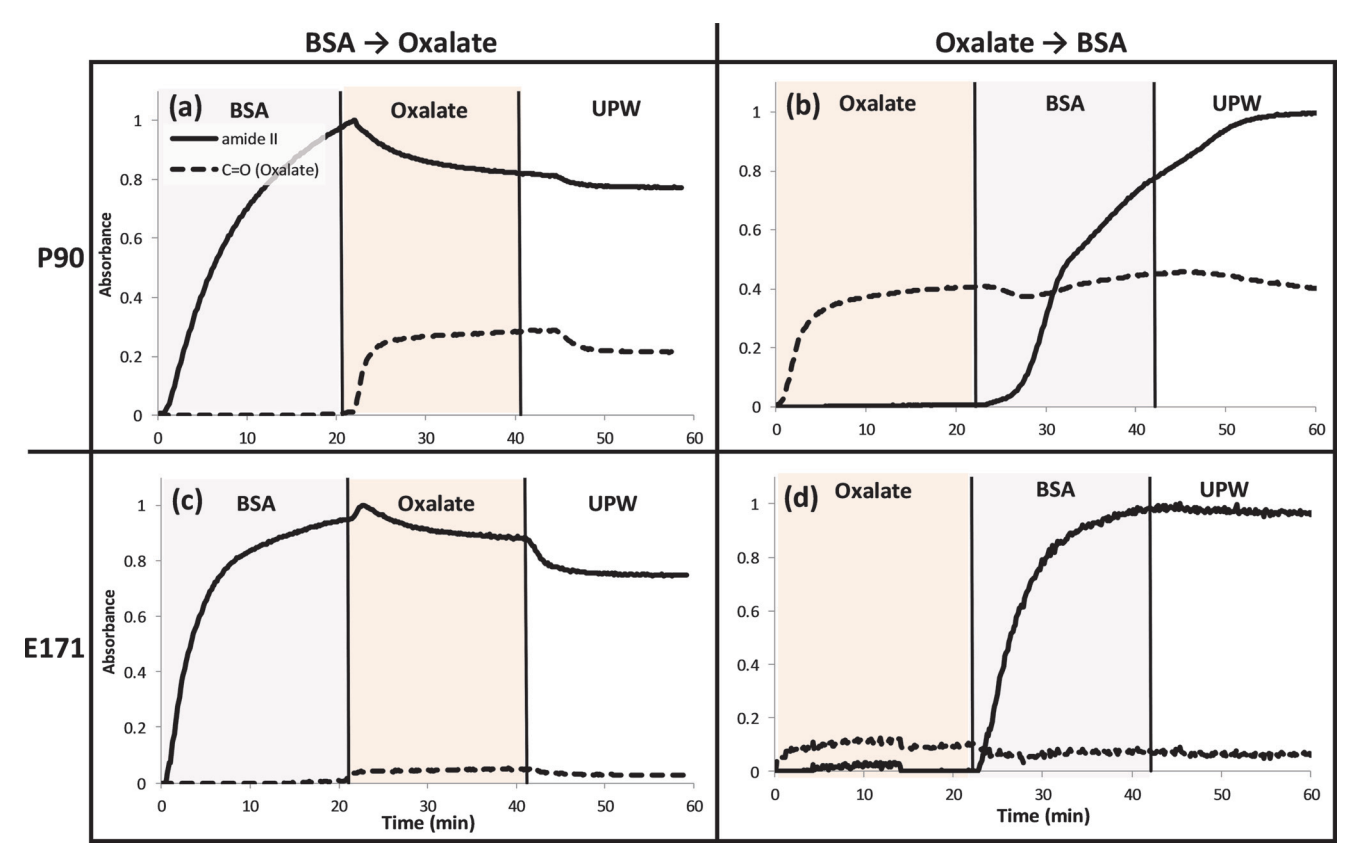


Fig. 4 Flow-through ATR-FTIR spectra (64 scans, 4 cm⁻¹) for BSA in the presence and absence of pre-formed oxalate layers on P90 (a and b) and E171 (c and d) films. All absorbances were normalized to the maximum value recorded. The amide II (1547 cm⁻¹) and C=O (1693 cm⁻¹ and 1699 cm⁻¹ for P90 and E171, respectively) peaks were selected for BSA and oxalate, respectively. Each dataset has three sequential phases: flow BSA/oxalate solution \rightarrow flow oxalate/BSA solution \rightarrow flow water. The vertical lines represent the time point at which each phase transitioned (e.g., 20 min). UPW is ultrapure water.

u. s⁻¹, respectively. The faster rate of adsorption onto E171 suggests the sorption behavior was dominated by physisorption compared to P90, which was likely a mixture of physi- and chemi-sorption. For P90 and E171, the addition of oxalate after BSA sorption caused BSA to partially desorb, which continued into the subsequent water phase. This indicates a fraction of BSA was weakly or reversibly adsorbed. The desorption was more apparent for E171, which confirms the sorption of BSA was dominated by physisorption mechanisms.

For the second scenario, with oxalate pre-adsorbed to the surface, the sorption kinetics and behavior of BSA changed for both P90 and E171 (Fig. 4 and S5a†). The initial rate for P90 (Fig. 4b) was 0.011 a.u. s⁻¹; however, the kinetics for P90 with pre-adsorbed oxalate were not straightforward and the use of a single initial rate is misleading. Instead, four distinct kinetic regions were observed (Fig. S5b†): (1) BSA adsorption was initially slow (0.011 a.u. s^{-1}); (2) the rate increased slightly (0.019 a.u. s^{-1}); (3) the rate increased (0.098 a.u. s^{-1}) to a similar rate as BSA adsorption on bare P90 (0.106 a.u. s^{-1}); (4) the rate slowed (0.037 a.u. s^{-1}), and then sorption continued into the water phase until reaching equilibrium. In the first two regions, BSA was presumably competing with oxalate for sorption sites, and oxalate was being displaced or rearranged as indicated by the decrease in the oxalate absorption intensity. In the third region, BSA adsorption preceded at a similar rate as to when no oxalate was present, suggesting oxalate had been partially displaced in favor of BSA. However, the absorption intensity of oxalate began increasing back to its original value precisely in this region even though there was no oxalate being added. This suggests oxalate was only being temporarily displaced or rearranged initially and then re-adsorbed simultaneously with BSA. In the last region, BSA sorption slowed as it approached saturation conditions. This suggests oxalate partially hindered the rate of adsorption of BSA but did not completely inhibit it. During the water phase, BSA was not desorbed as observed in the first scenario, rather it continued to adsorb, further providing evidence oxalate slows the adsorption kinetics of BSA with continued rearrangement and sorption. The adsorption behavior of BSA and oxalate in both scenarios is conceptualized in the schematic presented in Fig. 5.

For the adsorption of BSA onto E171 with pre-adsorbed oxalate (Fig. 4d), the initial rate was slower (0.141 a.u. s⁻¹) than in the absence of pre-adsorbed oxalate (i.e., Fig. 4b; 0.235 a.u. s⁻¹). No desorption of BSA from E171 occurred during the water phase, contrary to the first scenario, suggesting there is some degree of interaction between oxalate and BSA resulting Environmental Science: Nano Paper

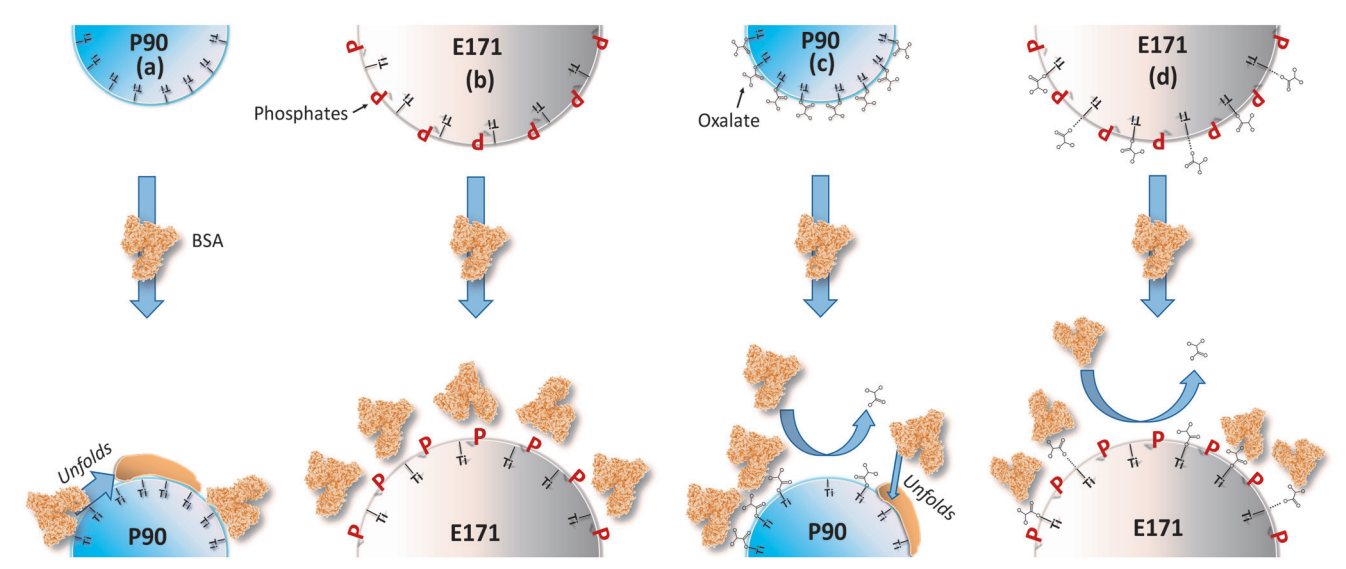


Fig. 5 A representative schematic of the adsorption behavior of BSA onto (left to right): bare P90, bare E171, P90 with pre-adsorbed oxalate, E171 with pre-adsorbed oxalate. The "P" represents phosphate groups. Figure is not to scale.

in irreversible sorption of BSA. Similar dynamic interactions between natural organic matter (NOM) and BSA were observed for TiO2, where the adsorption behavior was dependent on the "history" of exposure.32 When NOM and BSA were introduced simultaneously, an NOM-BSA complexed species adsorbed to TiO2 and multilayer sorption was inhibited. When the species were introduced sequentially (i.e., NOM and then BSA), the NOM dominated inner-layer adsorption with BSA populating the outer-layers of the macromolecular coating. Similar results have been reported regarding the competitive adsorption between humic acid and BSA onto TiO2.94 Humic acid adsorbed to TiO2 without displacing BSA due to non-specific hydrophobic interactions between adsorbate species.

The association of DOC (e.g., oxalate) with proteins has been contributed to π - π interactions, dipole-dipole bonding, electrostatic attraction, and hydrophobic interactions. 43,95-98 However, because both oxalate (p $K_{\rm a2}$ = 4.26) and BSA (p $H_{\rm zpc}$ = 4.8) are negatively charged at the experimental pH range (5.1-6.7), electrostatic attraction is not expected to be a major contributor. Additionally, the hydrophilic nature of oxalate will limit hydrophobic interactions. Therefore, dipole-dipole interactions (e.g., hydrogen bonds) and/or π - π interactions of C atoms of BSA and oxalate are presumably the main complexation mechanisms that overcome the electrostatic repulsion between BSA and oxalate, resulting in irreversible sorption of BSA.

For all scenarios, the sorption of BSA onto E171 was faster compared to P90 (Fig. S5†), presumably due to the physisorption-dominated mechanisms due to the phosphate bound to the surface of the TiO2. For both P90 and E171, the addition of oxalate to the system prior to BSA resulted in slower sorption kinetics of BSA, and its post addition resulted in the desorption and/or rearrangement of surface-adsorbed BSA. The rebound in oxalate adsorption after desorption suggests its displacement was only temporary. These results collectively indicate the "history" of the nanoparticle exposure can affect the kinetic and equilibrium conditions, and thus the resulting transport and bio-activity behavior of the nanoparticle. Consequently, accurate modeling of the protein corona formation will not be straightforward, and simply knowing the pristine or manufactured state of the nanoparticle or the environment it is exposed to (e.g., blood) will not be sufficient. Knowledge of the surface chemistry just prior to the protein corona formation will be critical.

The adsorption behavior of BSA and oxalate onto the TiO₂ ENMs was confirmed by analyzing the stability, HDS, and zeta potential (Table S2 and Fig. S6†), and by imaging with TEM (Fig. S7†). In water, P90 is stable but aggregated with an HDS of 279 \pm 3.4 nm. In the presence of BSA and oxalate, the HDS of P90 increased to 1116 \pm 75.6 nm and 2112 \pm 167 nm, respectively. A corresponding decrease in the zeta potential from positive to negative values was observed for each. In the presence of both BSA and oxalate, the HDS did not change significantly for P90 (302 \pm 4.2 nm), but the negative magnitude of the zeta potential increased. This suggests the BSA and oxalate complex adsorbs to P90 and stabilizes it through increased electrostatic repulsion. For E171, only the addition of BSA significantly altered the HDS (315 \pm 9.9 nm to 464 \pm 0.3 nm) and zeta potential (-27.3 \pm 2.9 mV to -0.2 \pm 0.8 mV). Results of the settling (i.e., stability) experiments in Fig. S6† showed only P90 with oxalate became unstable within 2 h, but both P90 and E171 with BSA became unstable within 24 h. The mixture of oxalate and BSA did not result in instability within 24 h, confirming the complexed BSA-oxalate species exhibits a different adsorption behavior than BSA or oxalate alone. This agrees with previous outcomes on the competitive sorption between NOM and BSA.32 TEM images confirmed the presence of BSA adsorbed to P90 and E171 (Fig. S7†). These outcomes collectively support the molecular-scale observations that protein adsorption, which alters the surface chemistry of the ENMs, is significantly affected by both the inherent surface chemistry of the ENM and the exposure to DOC.

Analysis of the secondary structure of BSA

The secondary structure of BSA was evaluated for the two scenarios described in the previous section to determine conformational changes occurring upon adsorption to TiO2 in the presence and absence of DOC (i.e., oxalate). The secondary structure of BSA was investigated using the amide I band $(\sim 1600-1700 \text{ cm}^{-1})$, which is sensitive to changes in secondary structure. 68,69 The amide I band of BSA was deconvoluted into β -sheets/turns, α -helices, random chains, extended chains/β-sheets, and side chain moieties (Fig. 6). Wavenumber ranges for each component of the BSA secondary structure are summarized in Table S1.†44,55,68,99-101 The $v_{as}(C=0)$ peak for oxalate was also fitted for relevant experimental results. The deconvoluted peak area percentages were determined as a function of the total amide I area to evaluate specific component changes with varying conditions (Table 2). The α -helix portion was used to evaluate perturbations and unfolding of the BSA structure. 68,102

The α -helix content of BSA on the bare IRE was 53.6% (*i.e.*, solution-phase). Upon adsorption to P90, the α -helix content decreased to 26.3%, which is in agreement with previous studies showing when proteins adsorb to surfaces they lose their helical structure due to strong interactions between the protein and surface (*e.g.*, chemisorption, hydrogen bonding). ^{70,76,103,104} In the presence of pre-adsorbed oxalate on P90, the α -helix content was comparatively

higher at 34.0%, indicating a lower degree of unfolding. Likewise, even when BSA was adsorbed first, the subsequent addition of oxalate to the system resulted in a higher α -helix content (32.9%) compared to the adsorption onto bare P90. These results suggest the displacement of BSA by oxalate allowed BSA to fold back into its α-helix structure, and this agrees with the kinetic data (i.e., Fig. 4) showing the desorption and/or rearrangement of BSA when oxalate was introduced. The unfolding of BSA α-helix has been suggested to proceed through β-sheets/chains and then to β -sheet/turns. ^{49,68} The total β -content (*i.e.*, extended and turns) for P90, P90 with pre-adsorbed oxalate, and P90 with adsorbed BSA and subsequent oxalate exposure was 40.9%, 30.9%, and 30.1%, respectively. This increase in β-content agrees with the decreasing trend observed for the α-helix content. The addition of a final water desorption phase for the latter two experiments did not significantly alter (i.e. <5%) the α -helix content (not shown, 34.5 and 35%, respectively). Thus, even though the desorption behavior differed between the two scenarios (i.e., Fig. 4a and b), water did not have a measurable effect on conformational changes. Collectively, these results suggest the presence of oxalate, whether it is pre-adsorbed or introduced after BSA adsorption, affects the conformational state of BSA on P90.

The α -helix and total β -content of BSA on E171 in the absence of oxalate was 54.9% and 31.5%, respectively. These

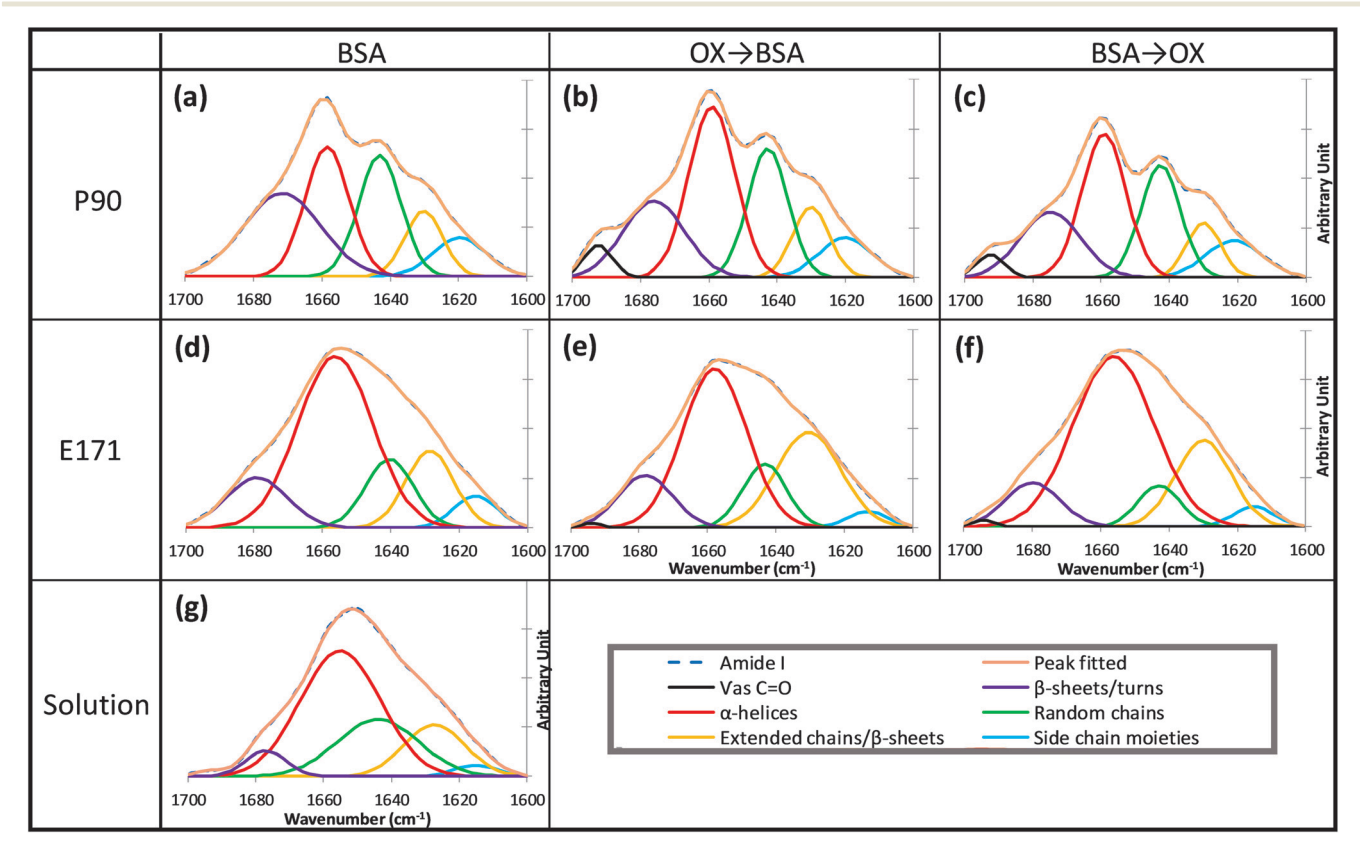


Fig. 6 The amide I band and secondary structure deconvoluted peaks of BSA for the different experimental scenarios involving (a–f) P90 and E171 and (g) the solution-phase with no TiO₂ or oxalate present. BSA is bovine serum albumin and OX is oxalate.

Table 2 Relative percent contribution of each secondary structure of BSA in solution phase and adsorbed onto P90 and E171. Goodness of fit was analyzed using χ^2 ; numerous fits were conducted, and the mean and standard deviation values are reported for all acceptable fits (i.e., $\chi^2 < 0.0002$). BSA is bovine serum albumin and OX is oxalate

Condition	Sample	Side chain moieties	Extended chains/β-sheets	Random chains	α-Helices	β-Sheets/turns	ν _{as} C=Ο
Solution Phase	BSA	2.9 ± 0.3	15.6 ± 2.8	22.1 ± 4.0	53.6 ± 4.9	5.8 ± 0.3	
P90	$\begin{array}{c} BSA \\ BSA \rightarrow OX \\ OX \rightarrow BSA \end{array}$	9.3 ± 0.1 10.6 ± 0.0 9.1 ± 0.1	11.4 ± 0.1 9.6 ± 0.0 10.9 ± 0.2	23.6 ± 0.0 23.0 ± 0.0 22.2 ± 0.1	26.3 ± 0.0 32.9 ± 0.1 34.0 ± 0.1	29.5 ± 0.0 20.5 ± 0.1 20.0 ± 0.1	3.3 ± 0.0 3.0 ± 0.0
E171	$\begin{array}{c} BSA \\ BSA \rightarrow OX \\ OX \rightarrow BSA \end{array}$	4.9 ± 0.6 3.5 ± 0.0 2.8 ± 0.1	19.4 ± 2.8 20.3 ± 0.0 27.4 ± 0.3	8.7 ± 3.3 7.3 ± 0.1 12.1 ± 0.3	54.9 ± 1.4 58.1 ± 0.1 44.7 ± 0.3	12.1 ± 0.3 10.2 ± 0.0 12.5 ± 0.1	 0.6 ± 0.0 0.4 ± 0.0

were similar to the solution-phase BSA contents (53.6%, 21.4%, respectively), suggesting BSA was weakly sorbed to E171, and the presence of phosphate groups on the TiO₂ surface deterred conformational changes. The presence of preadsorbed oxalate on E171 reduced the α-helix content to 44.7%, again indicating the ability of oxalate to induce conformational changes, as seen with P90. Interestingly, the α-helix content of BSA on both E171 and P90 pre-adsorbed with oxalate were markedly different (44.7% and 34%, respectively). This suggests the just the presence of oxalate alone does not determine the conformation of BSA, but rather the binding mechanism of oxalate to TiO2 affects how BSA conforms on the surface. The energetics of oxalate would be different since, as discussed previously, oxalate is strongly bound in the inner Stern layer to P90, but weakly bound in the outer Stern layer to E171 due to its phosphate coating. Thus, the phosphate coating appears to play a significant role in altering the sorption of oxalate and in turn the conformational changes of BSA upon adsorption.

Analysis of the sequential changes of the secondary structure using 2DCOS

Changes in the protein secondary structure upon adsorption are often rapid and simultaneous, making it difficult to determine the unfolding sequence. 2DCOS is a useful technique that can be used to deconvolute overlapping one-dimensional IR peaks that occur due to an external perturbation (i.e., time). 49,52,105,106 It was used herein to determine the sequence of secondary structural changes that occurred during the first minute of adsorption. Fig. 7 shows synchronous (real components) and asynchronous (imaginary components) 2DCOS plots and the spectrum analysis for the amide I secondary structures of BSA upon adsorption onto P90 and E171 in the absence and presence of oxalate. The sequential changes of the secondary structure of BSA upon adsorption was determined by the location and signs of cross peaks (ν 1, ν 2) in the synchronous and asynchronous spectral plots. When the sign of cross peaks is positive in the synchronous plot, both $\nu 1$ and $\nu 2$ increase or decrease simultaneously as adsorption progresses. In contrast, when the sign of cross peaks is negative, an opposing trend occurs, and $\nu 1$ increases while ν^2 decreases or *vice versa*. For the asynchronous plot, the cross peak shows a sequential change of spectral intensities that occurs as the external perturbation (time) is applied to the two waves, $\nu 1$ and $\nu 2$. In other words, variations in the dynamic changes observed for ν 1 and ν 2 can be seen from the asynchronous spectrum, where associated signs are expressed in red (+) and blue (-) (Fig. 7 and S8†). For the asynchronous cross peaks, there are four scenarios that can occur in the adsorption event and these are separated into the upper left and lower right regions of the spectrum plot (e.g., Fig. S8†): (1) if the cross peaks are located in the upper left (i.e., $\nu 1 < \nu 2$) and are positive (i.e., red), then the lower wavenumber, ν 1, occurs before the higher wavenumber, $\nu 2$; (2) if cross peaks are located in the lower right ($\nu 1 > \nu 2$) and are positive (red), then the higher wavenumber, $\nu 1$, occurs before the lower wavenumber, $\nu 2$; (3, 4) if the sign of the cross peaks is negative (blue), then the order is reversed for those regions.

At early time points (<1 min), an additional secondary structure peak was observed between 1690–1700 cm $^{-1}$, which has been identified as an additional β -sheets peak. 55,100,101 This β -sheets peak was distinguishable from the adjacent β -sheets/turns peak at early time points when the intensity of the β -sheets/turns peak was weak. As time progressed, the intensity the β -sheets/turns peak increased, while the β -sheets peak did not, and it became negligible in comparison. This additional β -sheets peak was not observed in the secondary structure peaks of BSA adsorbed onto E171.

For BSA adsorption to P90, the sequence of secondary structures observed immediately upon adsorption was random chains $\rightarrow \alpha$ -helix $\rightarrow \beta$ -sheets/turns \rightarrow side chain moieties $\rightarrow \beta$ -sheets (1631 cm⁻¹) $\rightarrow \beta$ -sheets (1693 cm⁻¹). In the presence of pre-adsorbed oxalate, the adsorption sequence of the BSA secondary structure was: α -helix $\rightarrow \beta$ -sheets/turns \rightarrow random chains \rightarrow side chain moieties $\rightarrow \beta$ -sheets (1629 cm⁻¹) $\rightarrow \beta$ -sheets (1695 cm⁻¹). Upon adsorption, the sequential changes of the secondary structure in the absence and presence of pre-adsorbed oxalate were similar with a general trend indicating the unfolding of BSA from α -helix to β -sheets.

For BSA adsorption to E171 in the absence of oxalate, the sequence of secondary structures observed upon adsorption was: β -sheets/turns \rightarrow random chains \rightarrow β -sheets \rightarrow α -helix \rightarrow side chain moieties. In the presence of pre-adsorbed

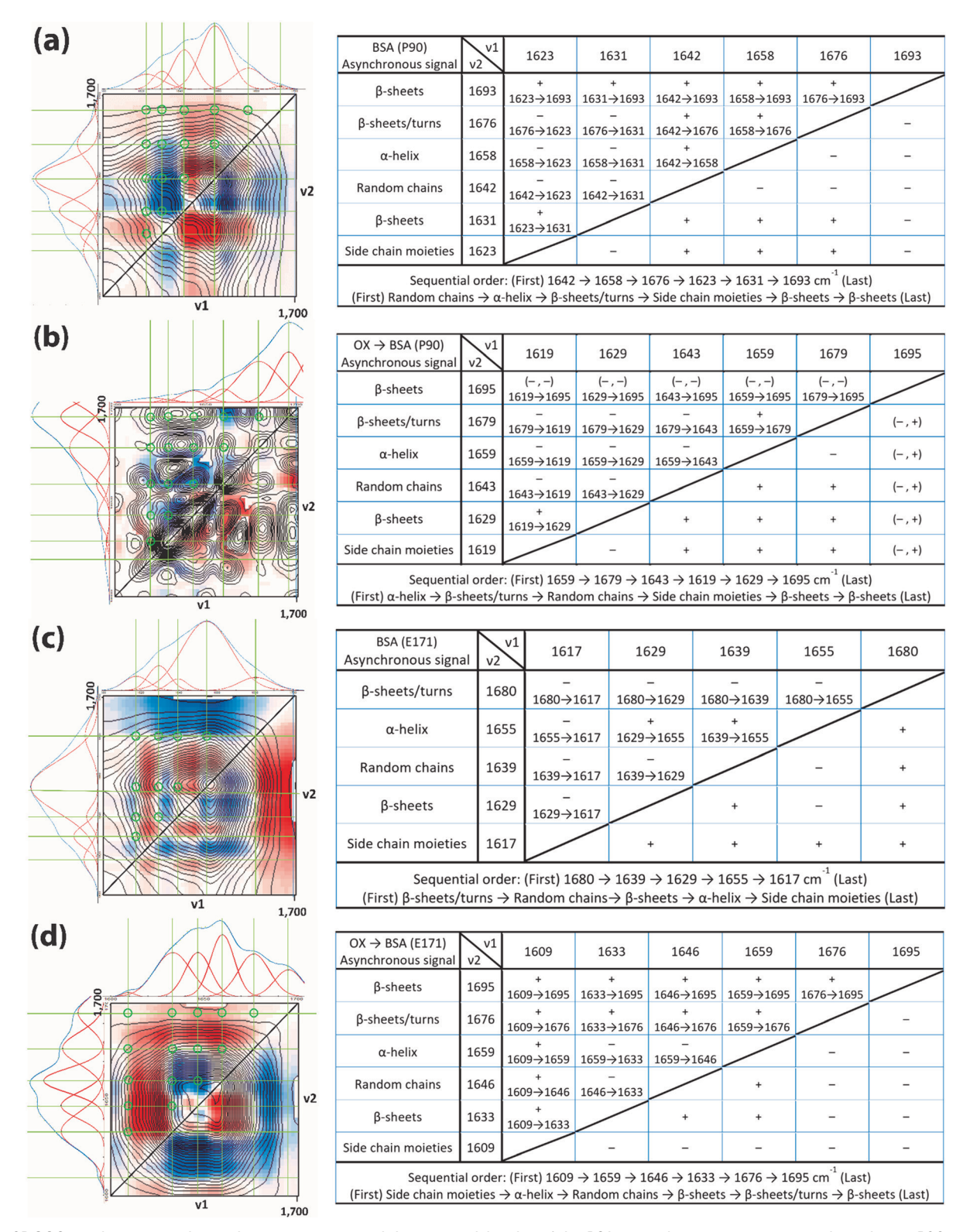


Fig. 7 2DCOS synchronous and asynchronous spectra and the sequential order of the BSA secondary structures upon adsorption to P90 and E171 in the presence and absence of pre-adsorbed oxalate. (a) BSA adsorption onto P90 in the absence of oxalate, (b) BSA adsorption onto P90 with pre-adsorbed oxalate, (c) BSA adsorption onto E171 in the absence of oxalate, (d) BSA adsorption onto E171 with pre-adsorbed oxalate. In the plots, the contour lines (black) and the colored regions (blue, red) represent the absorption intensities from synchronous and asynchronous spectrum, respectively. The IR peaks are the secondary structures of BSA. In the tables, the horizontal row and vertical column wavenumbers are ν1 and ν2, respectively. Except for (b), all synchronous secondary structure peaks were +, so the + or - shown in the tables are for the asynchronous spectra peaks. For (b), the parentheses represent the synchronous and asynchronous spectra, respectively, e.g., (-, -).

Environmental Science: Nano Paper

oxalate, the adsorption sequence of the BSA secondary structure was side chain moieties $\rightarrow \alpha$ -helix \rightarrow random chains \rightarrow β -sheets (1633 cm⁻¹) \rightarrow β -sheets/turns \rightarrow β -sheets (1695 cm⁻¹). In the absence of oxalate, the adsorption of BSA onto E171 was random and no clear unfolding trend was observed. As discussed previously, this suggests phosphate inhibits the binding of BSA to TiO2, and no mode of attraction (e.g., amino group attraction to Ti-OH₂⁺) allows BSA to approach the surface. This also agrees with the secondary structure analysis that showed minimal α -helix loss. In the presence of oxalate, the resulting sequence suggests unfolding occurred from α-helix to β-sheets/turns and this behavior was comparable to P90 in the presence of oxalate. The similar unfolding of BSA on P90 and E171 with pre-adsorbed oxalate indicates oxalate serves a specific role in the adsorption of BSA.

Conclusion

The inherent surface chemistry of ENMs is known to control the sorption of proteins, but little evidence has been provided on how the release of ENMs to the environment prior to biological uptake affects the protein corona formation. In this study, we used TRIS-ATR-FTIR to investigate the sorption of a model protein, BSA, onto two different types of TiO2 ENMs (catalyticgrade P90 and food-grade E171) in the presence and absence of a simple DOC molecule, oxalate. TiO2 is a commonly used model ENM in fate, transport, and toxicity studies because of its stability, widespread use, and low cost, but historically these studies have been conducted with catalytic grade TiO2 (e.g., P90) instead of the more prevalent food-grade TiO2, E171. Though a single protein (i.e., BSA) was used in this study, outcomes can be collectively used to understand protein corona formation. The inherent presence of phosphates on the surface of E171 will affect the sorption behavior of DOC and proteins, the presence of pre-adsorbed DOC on TiO2 will significantly change the adsorption behavior of proteins. The mechanism by which DOC is bound to TiO2 will impact the adsorption behavior of proteins significantly more than considering just the presence of DOC on the TiO2 surface.

Beyond medical applications, ENMs are unlikely to be taken up by organisms without first being exposed to natural (e.g., streams) or engineered systems (e.g., wastewater treatment plant). Thus, when considering the impact of the protein corona on the bioactivity of ENMs, not only must the "history" of the ENM be considered to understand how sorbed compounds affect its surface chemistry, but also the mechanism by which these compounds are bound to the ENM (e.g., chemisorbed), as this will impact the ensuing sorption kinetics and equilibrium behavior of proteins. Moving forward, using the outcomes of the simplistic systems used in this study as baseline knowledge, future studies should consider increasingly complex systems that have protein mixtures, more complex DOCs (e.g., humic acid), and the presence of other potentially complexing constituents (e.g., calcium), all while keeping in mind that the inherent ENM properties can affect these outcomes.

Conflicts of interest

There are no conflicts to declare.

Acknowledgements

This work was made possible through financial support provided by the University of Notre Dame and the National Science Foundation (CBET 1705770). The authors thank the Center for Environmental Science and Technology at Notre Dame (CEST) for the use of the DLS, PALS, and DRIFTS. We thank the Notre Dame Integrated Imaging Facility (NDIIF) for use of the TEM. Finally, we thank the Notre Dame Materials Characterization Facility (MCF) for use of the XPS.

References

- 1 T. Cedervall, I. Lynch, S. Lindman, T. Berggard, E. Thulin, H. Nilsson, K. A. Dawson and S. Linse, Understanding the nanoparticle-protein corona using methods to quantify exchange rates and affinities of proteins for nanoparticles, Proc. Natl. Acad. Sci. U. S. A., 2007, 104, 2050-2055.
- 2 M. Lundqvist, J. Stigler, G. Elia, I. Lynch, T. Cedervall and K. A. Dawson, Nanoparticle size and surface properties determine the protein corona with possible implications for biological impacts, Proc. Natl. Acad. Sci. U. S. A., 2008, 105, 14265-14270.
- 3 A. E. Nel, L. Madler, D. Velegol, T. Xia, E. M. V. Hoek, P. Somasundaran, F. Klaessig, V. Castranova and M. Thompson, Understanding biophysicochemical interactions at the nano-bio interface, Nat. Mater., 2009, 8, 543-557.
- 4 D. Walczyk, F. B. Bombelli, M. P. Monopoli, I. Lynch and K. A. Dawson, What the Cell "Sees" in Bionanoscience, J. Am. Chem. Soc., 2010, 132, 5761-5768.
- 5 C. C. Ge, J. F. Du, L. N. Zhao, L. M. Wang, Y. Liu, D. H. Li, Y. L. Yang, R. H. Zhou, Y. L. Zhao, Z. F. Chai and C. Y. Chen, Binding of blood proteins to carbon nanotubes reduces cytotoxicity, Proc. Natl. Acad. Sci. U. S. A., 2011, 108, 16968-16973.
- 6 W. B. Hu, C. Peng, M. Lv, X. M. Li, Y. J. Zhang, N. Chen, C. H. Fan and Q. Huang, Protein Corona-Mediated Mitigation of Cytotoxicity of Graphene Oxide, ACS Nano, 2011, 5, 3693-3700.
- 7 M. Lundqvist, J. Stigler, T. Cedervall, T. Berggard, M. B. Flanagan, I. Lynch, G. Elia and K. Dawson, The Evolution of the Protein Corona around Nanoparticles: A Test Study, ACS Nano, 2011, 5, 7503-7509.
- 8 M. P. Monopoli, D. Walczyk, A. Campbell, G. Elia, I. Lynch, F. B. Bombelli and K. A. Dawson, Physical-Chemical Aspects of Protein Corona: Relevance to in Vitro and in Vivo Biological Impacts of Nanoparticles, J. Am. Chem. Soc., 2011, 133, 2525-2534.
- 9 A. Lesniak, F. Fenaroli, M. R. Monopoli, C. Aberg, K. A. Dawson and A. Salvati, Effects of the Presence or Absence of a Protein Corona on Silica Nanoparticle Uptake and Impact on Cells, ACS Nano, 2012, 6, 5845-5857.

- 10 M. P. Monopoli, C. Aberg, A. Salvati and K. A. Dawson, Biomolecular coronas provide the biological identity of nanosized materials, *Nat. Nanotechnol.*, 2012, 7, 779–786.
- 11 C. D. Walkey and W. C. W. Chan, Understanding and controlling the interaction of nanomaterials with proteins in a physiological environment, *Chem. Soc. Rev.*, 2012, 41, 2780–2799.
- 12 A. Lesniak, A. Salvati, M. J. Santos-Martinez, M. W. Radomski, K. A. Dawson and C. Aberg, Nanoparticle Adhesion to the Cell Membrane and Its Effect on Nanoparticle Uptake Efficiency, J. Am. Chem. Soc., 2013, 135, 1438–1444.
- 13 S. R. Saptarshi, A. Duschl and A. L. Lopata, Interaction of nanoparticles with proteins: relation to bio-reactivity of the nanoparticle, *J. Nanobiotechnol.*, 2013, 11, 12.
- 14 S. Tenzer, D. Docter, J. Kuharev, A. Musyanovych, V. Fetz, R. Hecht, F. Schlenk, D. Fischer, K. Kiouptsi, C. Reinhardt, K. Landfester, H. Schild, M. Maskos, S. K. Knauer and R. H. Stauber, Rapid formation of plasma protein corona critically affects nanoparticle pathophysiology, *Nat. Nanotechnol.*, 2013, 8, 772–U1000.
- 15 P. Del Pino, B. Pelaz, Q. Zhang, P. Maffre, G. U. Nienhaus and W. J. Parak, Protein corona formation around nanoparticles from the past to the future, *Mater. Horiz.*, 2014, 1, 301–313.
- 16 D. Docter, C. Bantz, D. Westmeier, H. J. Galla, Q. B. Wang, J. C. Kirkpatrick, P. Nielsen, M. Maskos and R. H. Stauber, The protein corona protects against size- and dosedependent toxicity of amorphous silica nanoparticles, *Beilstein J. Nanotechnol.*, 2014, 5, 1380–1392.
- 17 C. Gunawan, M. Lim, C. P. Marquis and R. Amal, Nanoparticle-protein corona complexes govern the biological fates and functions of nanoparticles, *J. Mater. Chem. B*, 2014, 2, 2060–2083.
- 18 L. Treuel, S. Brandholt, P. Maffre, S. Wiegele, L. Shang and G. U. Nienhaus, Impact of Protein Modification on the Protein Corona on Nanoparticles and Nanoparticle-Cell Interactions, ACS Nano, 2014, 8, 503–513.
- 19 C. D. Walkey, J. B. Olsen, F. Y. Song, R. Liu, H. B. Guo, D. W. H. Olsen, Y. Cohen, A. Emili and W. C. W. Chan, Protein Corona Fingerprinting Predicts the Cellular Interaction of Gold and Silver Nanoparticles, ACS Nano, 2014, 8, 2439–2455.
- 20 G. Caracciolo, S. Palchetti, V. Colapicchioni, L. Digiacomo, D. Pozzi, A. L. Capriotti, G. La Barbera and A. Lagana, Stealth Effect of Biomolecular Corona on Nanoparticle Uptake by Immune Cells, *Langmuir*, 2015, 31, 10764–10773.
- 21 X. J. Cheng, X. Tian, A. Q. Wu, J. X. Li, J. Tian, Y. Chong, Z. F. Chai, Y. L. Zhao, C. Y. Chen and C. C. Ge, Protein Corona Influences Cellular Uptake of Gold Nanoparticles by Phagocytic and Nonphagocytic Cells in a Size-Dependent Manner, ACS Appl. Mater. Interfaces, 2015, 7, 20568–20575.
- 22 D. Docter, D. Westmeier, M. Markiewicz, S. Stolte, S. K. Knauer and R. H. Stauber, The nanoparticle biomolecule corona: lessons learned challenge accepted?, *Chem. Soc. Rev.*, 2015, 44, 6094-6121.

- 23 P. Foroozandeh and A. A. Aziz, Merging Worlds of Nanomaterials and Biological Environment: Factors Governing Protein Corona Formation on Nanoparticles and Its Biological Consequences, *Nanoscale Res. Lett.*, 2015, 10, 12.
- 24 C. C. Ge, J. Tian, Y. L. Zhao, C. Y. Chen, R. H. Zhou and Z. F. Chai, Towards understanding of nanoparticle-protein corona, *Arch. Toxicol.*, 2015, 89, 519–539.
- 25 R. Liu, W. Jiang, C. D. Walkey, W. C. W. Chan and Y. Cohen, Prediction of nanoparticles-cell association based on corona proteins and physicochemical properties, *Nanoscale*, 2015, 7, 9664–9675.
- 26 D. Pozzi, G. Caracciolo, L. Digiacomo, V. Colapicchioni, S. Palchetti, A. L. Capriotti, C. Cavaliere, R. Z. Chiozzi, A. Puglisi and A. Lagana, The biomolecular corona of nanoparticles in circulating biological media, *Nanoscale*, 2015, 7, 13958–13966.
- 27 F. Gottschalk, T. Sonderer, R. W. Scholz and B. Nowack, Possibilities and limitations of modeling environmental exposure to engineered nanomaterials by probabilistic material flow analysis, *Environ. Toxicol. Chem.*, 2010, 29, 1036–1048.
- 28 A. A. Keller, S. McFerran, A. Lazareva and S. Suh, Global life cycle releases of engineered nanomaterials, *J. Nanopart. Res.*, 2013, 15, 1692.
- 29 V. M. Gun'ko, L. I. Mikhalovska, P. E. Tomlins and S. V. Mikhalovsky, Competitive adsorption of macromolecules and real-time dynamics of Vroman-like effects, *Phys. Chem. Chem. Phys.*, 2011, 13, 4476–4485.
- 30 D.-H. Tsai, M. Davila-Morris, F. W. DelRio, S. Guha, M. R. Zachariah and V. A. Hackley, Quantitative Determination of Competitive Molecular Adsorption on Gold Nanoparticles Using Attenuated Total Reflectance–Fourier Transform Infrared Spectroscopy, *Langmuir*, 2011, 27, 9302–9313.
- 31 Z. Xu and V. H. Grassian, Bovine Serum Albumin Adsorption on TiO2 Nanoparticle Surfaces: Effects of pH and Coadsorption of Phosphate on Protein–Surface Interactions and Protein Structure, *J. Phys. Chem. C*, 2017, 121, 21763–21771.
- 32 S. Shakiba, A. Hakimian, L. R. Barco and S. M. Louie, Dynamic Intermolecular Interactions Control Adsorption from Mixtures of Natural Organic Matter and Protein onto Titanium Dioxide Nanoparticles, *Environ. Sci. Technol.*, 2018, 52, 14158–14168.
- 33 M. Kitis, J. E. Kilduff and T. Karanfil, Isolation of dissolved organic matter (dom) from surface waters using reverse osmosis and its impact on the reactivity of dom to formation and speciation of disinfection by-products, *Water Res.*, 2001, 35, 2225–2234.
- 34 J. S. Gaffney, N. A. Marley and S. B. Clark, *Humic and Fulvic Acids and Organic Colloidal Materials in the Environment*, American Chemical Society, 1996.
- 35 H. K. Tan, *Humic Matter in Soil and the Environment:* Principles and Controversies, CRC Press, 2nd edn, 2014.
- 36 C. Jiang, G. R. Aiken and H. Hsu-Kim, Effects of Natural Organic Matter Properties on the Dissolution Kinetics of Zinc Oxide Nanoparticles, *Environ. Sci. Technol.*, 2015, 49, 11476–11484.

- 37 R. Grillo, A. H. Rosa and L. F. Fraceto, Engineered nanoparticles and organic matter: A review of the state-of-the-art, *Chemosphere*, 2015, 119, 608–619.
- 38 M.-H. Shen, Y.-G. Yin, A. Booth and J.-F. Liu, Effects of molecular weight-dependent physicochemical heterogeneity of natural organic matter on the aggregation of fullerene nanoparticles in mono- and di-valent electrolyte solutions, *Water Res.*, 2015, 71, 11–20.
- 39 B. Gu, J. Schmitt, Z. Chen, L. Liang and J. F. McCarthy, Adsorption and desorption of different organic matter fractions on iron oxide, *Geochim. Cosmochim. Acta*, 1995, 59, 219–229.
- 40 A. M. Vindedahl, M. S. Stemig, W. A. Arnold and R. L. Penn, Character of Humic Substances as a Predictor for Goethite Nanoparticle Reactivity and Aggregation, *Environ. Sci. Technol.*, 2016, 50, 1200–1208.
- 41 A. M. Vindedahl, J. H. Strehlau, W. A. Arnold and R. L. Penn, Organic matter and iron oxide nanoparticles: aggregation, interactions, and reactivity, *Environ. Sci.: Nano*, 2016, 3, 494–505.
- 42 E. M. Hotze, S. M. Louie, S. Lin, M. R. Wiesner and G. V. Lowry, Nanoparticle core properties affect attachment of macromolecule-coated nanoparticles to silica surfaces, *Environ. Chem.*, 2014, 11, 257–267.
- 43 J. E. Tomaszewski, M. Madliger, J. A. Pedersen, R. P. Schwarzenbach and M. Sander, Adsorption of Insecticidal Cry1Ab Protein to Humic Substances. 2. Influence of Humic and Fulvic Acid Charge and Polarity Characteristics, *Environ. Sci. Technol.*, 2012, 46, 9932–9940.
- 44 B. E. Givens, Z. Xu, J. Fiegel and V. H. Grassian, Bovine serum albumin adsorption on SiO2 and TiO2 nanoparticle surfaces at circumneutral and acidic pH: A tale of two nano-bio surface interactions, *J. Colloid Interface Sci.*, 2017, 493, 334–341.
- 45 A. Jedlovszky-Hajdú, F. B. Bombelli, M. P. Monopoli, E. Tombácz and K. A. Dawson, Surface Coatings Shape the Protein Corona of SPIONs with Relevance to Their Application in Vivo, *Langmuir*, 2012, 28, 14983–14991.
- 46 I. A. Mudunkotuwa and V. H. Grassian, Biological and environmental media control oxide nanoparticle surface composition: the roles of biological components (proteins and amino acids), inorganic oxyanions and humic acid, *Environ. Sci.: Nano*, 2015, 2, 429–439.
- 47 I. A. Mudunkotuwa, A. A. Minshid and V. H. Grassian, ATR-FTIR spectroscopy as a tool to probe surface adsorption on nanoparticles at the liquid-solid interface in environmentally and biologically relevant media, *Analyst*, 2014, 139, 870–881.
- 48 K. Doudrick, O. Monzón, A. Mangonon, K. Hristovski and P. Westerhoff, Nitrate Reduction in Water Using Commercial Titanium Dioxide Photocatalysts (P25, P90, and Hombikat UV100), *J. Environ. Eng.*, 2012, 138, 852–861.
- 49 M. P. Schmidt and C. E. Martínez, Kinetic and Conformational Insights of Protein Adsorption onto Montmorillonite Revealed Using in Situ ATR-FTIR/2D-COS, *Langmuir*, 2016, 32, 7719–7729.

- 50 D.-H. Tsai, F. W. DelRio, A. M. Keene, K. M. Tyner, R. I. MacCuspie, T. J. Cho, M. R. Zachariah and V. A. Hackley, Adsorption and Conformation of Serum Albumin Protein on Gold Nanoparticles Investigated Using Dimensional Measurements and in Situ Spectroscopic Methods, *Langmuir*, 2011, 27, 2464–2477.
- 51 M. Wojdyr, Fityk: a general-purpose peak fitting program, *J. Appl. Crystallogr.*, 2010, 43, 1126–1128.
- 52 I. Noda and Y. Ozaki, Two-Dimensional Correlation Spectroscopy: Applications in Vibrational and Optical Spectroscopy, WILEY, 2004.
- 53 Y. Yang, K. Doudrick, X. Bi, K. Hristovski, P. Herckes, P. Westerhoff and R. Kaegi, Characterization of Food-Grade Titanium Dioxide: The Presence of Nanosized Particles, *Environ. Sci. Technol.*, 2014, 48, 6391–6400.
- 54 J. J. Faust, K. Doudrick, Y. Yang, P. Westerhoff and D. G. Capco, Food grade titanium dioxide disrupts intestinal brush border microvilli in vitro independent of sedimentation, *Cell Biol. Toxicol.*, 2014, 30, 169–188.
- 55 A. Barth, Infrared spectroscopy of proteins, *Biochim. Biophys. Acta, Bioenerg.*, 2007, 1767, 1073–1101.
- 56 S. Benkoula, O. Sublemontier, M. Patanen, C. Nicolas, F. Sirotti, A. Naitabdi, F. Gaie-Levrel, E. Antonsson, D. Aureau, F.-X. Ouf, S.-I. Wada, A. Etcheberry, K. Ueda and C. Miron, Water adsorption on TiO2 surfaces probed by soft X-ray spectroscopies: bulk materials vs. isolated nanoparticles, *Sci. Rep.*, 2015, 5, 15088.
- 57 P. A. Connor, K. D. Dobson and A. J. McQuillan, Infrared Spectroscopy of the TiO2/Aqueous Solution Interface, *Langmuir*, 1999, 15, 2402–2408.
- 58 T. H. Yoon, S. B. Johnson, C. B. Musgrave and G. E. Brown, Adsorption of organic matter at mineral/water interfaces: I. ATR-FTIR spectroscopic and quantum chemical study of oxalate adsorbed at boehmite/water and corundum/water interfaces, *Geochim. Cosmochim. Acta*, 2004, 68, 4505–4518.
- 59 S. J. Hug and D. Bahnemann, Infrared spectra of oxalate, malonate and succinate adsorbed on the aqueous surface of rutile, anatase and lepidocrocite measured with in situ ATR-FTIR, J. Electron Spectrosc. Relat. Phenom., 2006, 150, 208-219.
- 60 A. D. Weisz, L. G. Rodenas, P. J. Morando, A. E. Regazzoni and M. A. Blesa, FTIR study of the adsorption of single pollutants and mixtures of pollutants onto titanium dioxide in water: oxalic and salicylic acids, *Catal. Today*, 2002, 76, 103–112.
- 61 M. A. Elsheikh, Z. Abidin, N. Matsue and T. Henmi, Competitive Adsorption of Oxalate and Phosphate on Allophane at Low Concentration, *Clay Sci.*, 2008, 13, 181–188.
- 62 C. N. Guppy, N. W. Menzies, P. W. Moody and F. P. C. Blamey, Competitive sorption reactions between phosphorus and organic matter in soil: a review, *Aust. J. Soil Res.*, 2005, 43, 189–202.
- 63 S. Nagarajah, A. M. Posner and J. P. Quirk, Competitive Adsorption of Phosphate with Polygalacturonate and other Organic Anions on Kaolinite and Oxide Surfaces, *Nature*, 1970, 228, 83.

- 64 M. Long, J. Brame, F. Qin, J. Bao, Q. Li and P. J. J. Alvarez, Phosphate Changes Effect of Humic Acids on TiO2 Photocatalysis: From Inhibition to Mitigation of Electron– Hole Recombination, *Environ. Sci. Technol.*, 2017, 51, 514–521.
- 65 P. A. Connor and A. J. McQuillan, Phosphate Adsorption onto TiO2 from Aqueous Solutions: An in Situ Internal Reflection Infrared Spectroscopic Study, *Langmuir*, 1999, 15, 2916–2921.
- 66 L. A. Buchanan and A. El-Ghannam, Effect of bioactive glass crystallization on the conformation and bioactivity of adsorbed proteins, *J. Biomed. Mater. Res.*, Part A, 2009, 93, 537–546.
- 67 S. J. McClellan and E. I. Franses, Adsorption of bovine serum albumin at solid/aqueous interfaces, *Colloids Surf.*, *A*, 2005, 260, 265–275.
- 68 P. Roach, D. Farrar and C. C. Perry, Interpretation of Protein Adsorption: Surface-Induced Conformational Changes, J. Am. Chem. Soc., 2005, 127, 8168–8173.
- 69 A. Barth and C. Zscherp, What vibrations tell about proteins, *Q. Rev. Biophys.*, 2002, 35, 369–430.
- 70 L. Song, K. Yang, W. Jiang, P. Du and B. Xing, Adsorption of bovine serum albumin on nano and bulk oxide particles in deionized water, *Colloids Surf.*, B, 2012, 94, 341–346.
- 71 B. Liedberg, B. Ivarsson and I. Lundström, Fourier transform infrared reflection absorption spectroscopy (FT-IRAS) of fibrinogen adsorbed on metal and metal oxide surfaces, *J. Biochem. Biophys. Methods*, 1984, 9, 233–243.
- 72 J. Lipkowski, Chapter One Biomimetic Membrane Supported at a Metal Electrode Surface: A Molecular View, Academic Press, 2014.
- 73 N. G. Hoogeveen, M. A. C. Stuart and G. J. Fleer, Polyelectrolyte Adsorption on Oxides: I. Kinetics and Adsorbed Amounts, J. Colloid Interface Sci., 1996, 182, 133–145.
- 74 K. Kubiak-Ossowska and P. A. Mulheran, What Governs Protein Adsorption and Immobilization at a Charged Solid Surface?, *Langmuir*, 2010, 26, 7690–7694.
- 75 A. Márquez, T. Berger, A. Feinle, N. Hüsing, M. Himly, A. Duschl and O. Diwald, Bovine Serum Albumin Adsorption on TiO2 Colloids: The Effect of Particle Agglomeration and Surface Composition, *Langmuir*, 2017, 33, 2551–2558.
- 76 W. Norde and J. Lyklema, The adsorption of human plasma albumin and bovine pancreas ribonuclease at negatively charged polystyrene surfaces: I. Adsorption isotherms. Effects of charge, ionic strength, and temperature, J. Colloid Interface Sci., 1978, 66, 257–265.
- 77 W. Norde, Driving forces for protein adsorption at solid surfaces, *Macromol. Symp.*, 1996, **103**, 5–18.
- 78 W. Norde and J. Lyklema, The adsorption of human plasma albumin and bovine pancreas ribonuclease at negatively charged polystyrene surfaces: II. Hydrogen ion titrations, J. Colloid Interface Sci., 1978, 66, 266–276.
- 79 W. Norde and J. Lyklema, The adsorption of human plasma albumin and bovine pancreas ribonuclease at negatively

- charged polystyrene surfaces: III. Electrophoresis, *J. Colloid Interface Sci.*, 1978, 66, 277–284.
- 80 W. Norde and J. Lyklema, The adsorption of human plasma albumin and bovine pancreas ribonuclease at negatively charged polystyrene surfaces: IV. The charge distribution in the adsorbed state, *J. Colloid Interface Sci.*, 1978, 66, 285–294.
- 81 W. Norde and J. Lyklema, The adsorption of human plasma albumin and bovine pancreas ribonuclease at negatively charged polystyrene surfaces: V. Microcalorimetry, *J. Colloid Interface Sci.*, 1978, 66, 295–302.
- 82 W. Norde and J. Lyklema, Thermodynamics of protein adsorption. Theory with special reference to the adsorption of human plasma albumin and bovine pancreas ribonuclease at polystyrene surfaces, *J. Colloid Interface Sci.*, 1979, 71, 350–366.
- 83 K. Wang, C. Zhou, Y. Hong and X. Zhang, A review of protein adsorption on bioceramics, *Interface Focus*, 2012, 2, 259.
- 84 Y. L. Jeyachandran, E. Mielczarski, B. Rai and J. A. Mielczarski, Quantitative and Qualitative Evaluation of Adsorption/Desorption of Bovine Serum Albumin on Hydrophilic and Hydrophobic Surfaces, *Langmuir*, 2009, 25, 11614–11620.
- 85 Z. Yang and C. Zhang, Adsorption/desorption behavior of protein on nanosized hydroxyapatite coatings: A quartz crystal microbalance study, *Appl. Surf. Sci.*, 2009, 255, 4569–4574.
- 86 K. D. Dobson and A. J. McQuillan, In situ infrared spectroscopic analysis of the adsorption of aliphatic carboxylic acids to TiO2, ZrO2, Al2O3, and Ta2O5 from aqueous solutions, *Spectrochim. Acta, Part A*, 1999, 55, 1395–1405.
- 87 H. B. Stuart, *Infrared Spectroscopy: Fundamentals and Applications*, WILEY, 2005.
- 88 A. Baral, L. Satish, D. P. Das, H. Sahoo and M. K. Ghosh, Construing the interactions between MnO2 nanoparticle and bovine serum albumin: insight into the structure and stability of a protein–nanoparticle complex, *New J. Chem.*, 2017, 41, 8130–8139.
- 89 C. Aharoni and F. C. Tompkins, *Kinetics of Adsorption and Desorption and the Elovich Equation*, Academic Press, 1970.
- 90 Y. S. Ho and G. McKay, Pseudo-second order model for sorption processes, *Process Biochem.*, 1999, 34, 451–465.
- 91 L. Largitte and R. Pasquier, A review of the kinetics adsorption models and their application to the adsorption of lead by an activated carbon, *Chem. Eng. Res. Des.*, 2016, 109, 495–504.
- 92 Y. Xiao, J. Azaiez and J. M. Hill, Erroneous Application of Pseudo-Second-Order Adsorption Kinetics Model: Ignored Assumptions and Spurious Correlations, *Ind. Eng. Chem. Res.*, 2018, 57, 2705–2709.
- 93 A. Pavlatou and N. A. Polyzopoulos, The role of diffusion in the kinetics of phosphate desorption: the relevance of the Elovich equation, *J. Soil Sci.*, 1988, 39, 425–436.
- 94 H. Wu, N. I. Gonzalez-Pech and V. H. Grassian, Displacement reactions between environmentally and biologically relevant ligands on TiO2 nanoparticles:

Environmental Science: Nano Paper

- insights into the aging of nanoparticles in the environment, Environ. Sci.: Nano, 2019, 6, 489-504.
- 95 M. Bayrakci, O. Gezici, S. Z. Bas, M. Ozmen and E. Maltas, Novel humic acid-bonded magnetite nanoparticles for protein immobilization, Mater. Sci. Eng., C, 2014, 42, 546-552.
- Y. Li, W. Tan, L. K. Koopal, M. Wang, F. Liu and W. Norde, Influence of Soil Humic and Fulvic Acid on the Activity and Stability of Lysozyme and Urease, Environ. Sci. Technol., 2013, 47, 5050-5056.
- 97 W. F. Tan, L. K. Koopal and W. Norde, Interaction between Humic Acid and Lysozyme, Studied by Dynamic Light Scattering and Isothermal Titration Calorimetry, Environ. Sci. Technol., 2009, 43, 591-596.
- 98 J. E. Tomaszewski, R. P. Schwarzenbach and M. Sander, Protein Encapsulation by Humic Substances, Environ. Sci. Technol., 2011, 45, 6003-6010.
- 99 P. Roach, D. Farrar and C. C. Perry, Surface Tailoring for Controlled Protein Adsorption: Effect of Topography at the Nanometer Scale and Chemistry, I. Am. Chem. Soc., 2006, 128, 3939-3945.
- 100 R. I. Litvinov, D. A. Faizullin, Y. F. Zuev and J. W. Weisel, The α-Helix to β-Sheet Transition in Stretched and Compressed Hydrated Fibrin Clots, Biophys. J., 2012, 103, 1020-1027.

- 101 A. Adamiano, G. Lesci Isidoro, D. Fabbri and N. Roveri, Adsorption of bovine serum albumin onto synthetic Fedoped geomimetic chrysotile, J. R. Soc., Interface, 2015, 12, 20150186.
- 102 B. E. Givens, N. D. Diklich, J. Fiegel and V. H. Grassian, Adsorption of bovine serum albumin silicon dioxide nanoparticles: Impact of pН nanoparticle-protein interactions. Biointerphases, 2017, 12, 02D404.
- 103 H. Pan, M. Qin, W. Meng, Y. Cao and W. Wang, How Do Proteins Unfold upon Adsorption on Nanoparticle Surfaces?, Langmuir, 2012, 28, 12779-12787.
- 104 A. Sethuraman, G. Vedantham, T. Imoto, T. Przybycien and G. Belfort, Protein unfolding at interfaces: Slow dynamics of α -helix to β -sheet transition, *Proteins: Struct., Funct., Bio*inf., 2004, 56, 669-678.
- 105 I. Noda, Vibrational two-dimensional correlation spectroscopy (2DCOS) study of proteins, Spectrochim. Acta, Part A, 2017, 187, 119-129.
- 106 V. A. Shashilov and I. K. Lednev, Two-dimensional correlation Raman spectroscopy for characterizing protein structure and dynamics, J. Raman Spectrosc., 2009, 40, 1749-1758.